

Open-Path Ghost Spectroscopy Based on Hadamard Modulation

Jianing Zhao, Fengyuan Liu , Zhenzhou Tang , *Member, IEEE*, and Shilong Pan , *Senior Member, IEEE*

Abstract—In order to achieve spectral detection in free space, an open-path ghost spectroscopy (GS) based on complementary Hadamard modulation is proposed. In the proposed system, a programmable spectral filter is used to modulate a series of Hadamard patterns to a broadband signal provided by an amplified spontaneous emission (ASE) source, and the spectrum-under-test is recovered by cross correlation between the power measured by an optical power meter and the Hadamard patterns. Both the simulation and experiment are carried out, and the highest spectral resolution up to 0.126 nm is achieved. Furthermore, the detection performance of the GS in a designed strong turbulence path is also demonstrated, which shows that the proposed GS is a promising solution to recover the optical spectrum in the condition of weak light and strong turbulence in the open path.

Index Terms—Computational spectral ghost imaging, Hadamard modulation, open-path ghost spectroscopy.

I. INTRODUCTION

IN THE past few years, open-path spectroscopy has been provided an effective means in monitoring urban greenhouse gas emissions, fire warning in the depopulated zone, and crop pest and disease control [1], which are typically realized by dual-frequency comb spectroscopy [2], [3], [4] or open-path Fourier transform infrared spectroscopy technique [5]. However, limited to the randomness and disorder of the spatial link, the atmospheric turbulence effect will affect the propagation of light, leading to the decline of useful information of the target, as well as the effective acquisition of the target spectral information [6]. In order to combat the atmospheric turbulence induced by open path, the common method of the high precision spectroscopy is to increase the refresh rate of the light source, which cannot fundamentally solve the problem but leads to the increase of the system complexity [2]. At the same time, the demand of high

Manuscript received 23 March 2022; revised 19 July 2022; accepted 8 August 2022. Date of publication 15 August 2022; date of current version 4 November 2022. This work was supported in part by the National Key R&D Program of China under Grant 2020YFB1805704, in part by the National Natural Science Foundation of China under Grant 62001218, in part by the National Natural Science Foundation of Jiangsu Province under Grant BK20200436, in part by the 2021 Jiangsu Shuangchuang Talent Program under Grant JSSCBS20210174, and in part by Postgraduate Research & Practice Innovation Program of Jiangsu Province under Grant KYCX21_0219. (Corresponding authors: Zhenzhou Tang; Shilong Pan).

The authors are with the Key Laboratory of Radar Imaging and Microwave Photonics, Ministry of Education, Nanjing University of Aeronautics and Astronautics, Nanjing 210016, China (e-mail: jianing@nuaa.edu.cn; liufengyuan@nuaa.edu.cn; tangzhzh@nuaa.edu.cn; pans@nuaa.edu.cn).

Color versions of one or more figures in this article are available at <https://doi.org/10.1109/JLT.2022.3198556>.

Digital Object Identifier 10.1109/JLT.2022.3198556

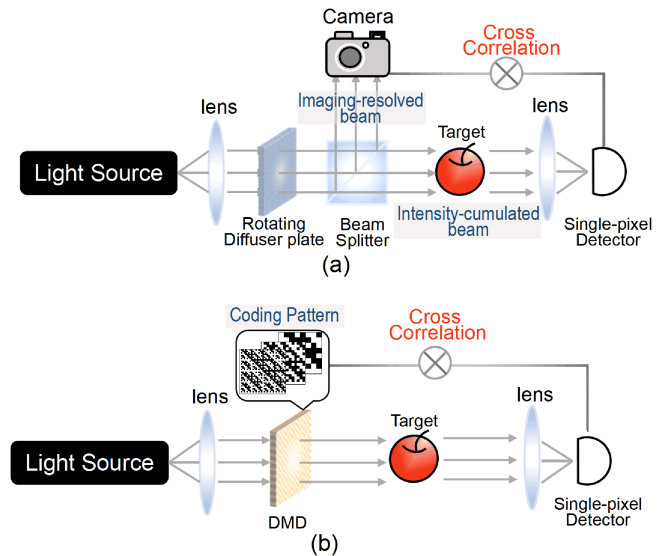


Fig. 1. Comparison between traditional GI and computational GI system. (a) Setup of traditional GI system. (b) Setup of computational GI system. DMD, digital mirror device.

sensitivity detector in specific frequency bands also limits its extension to longer wavelength such as infrared and mid-infrared regions.

To solve the problem, ghost imaging (GI) technique is regarded as a promising method. Originated from the quantum entanglement phenomenon [7], GI is an indirect technique that retrieves the object image by correlation measurements of light field intensity with a single-pixel detector. As can be seen from Fig. 1(a), through the correlation between the imaging-resolved beam with only field distribution information (without object information) and the intensity-cumulated beam with object information, the image can be retrieved by the summing of incident field that weighted by the integrated intensity from the objects. In order to break the bandwidth limitation of high-precision detectors [8], [9], [10] and to retrieve the object with less detection [11], [12], [13], the classical two-beam GI system shown in Fig. 1(a) can be upgraded to a one-beam computational GI system by illuminating the object with quadrature encoding structured light field based on like Hadamard matrix or Fourier basis patterns, as shown in Fig. 1(b). In the computational GI system, the image of the object is obtained by correlating the coding patterns depicted on digital mirror device with measured intensities. The reason why GI can be applied to the open-path applications is its distinct properties of resisting object light

attenuation and channel interference. Originally, the GI technique is applied in the space domain to achieve turbulence-free imaging. For example, in [14], [15], the maximum depth and corresponding imaging results of GI in different scattering media (turbidity solution and chicken tissue) are respectively investigated, which confirm the imaging ability of GI under weak light conditions. [16], [17] achieve a correlation imaging under the influence of atmospheric turbulence, which show a weak influence of atmospheric turbulence on GI. [18], [19] extend the experiment environment to the long distance, proving again that GI has better robustness than traditional imaging methods under the atmospheric turbulence.

Thanks to the well-known duality between space, time and frequency, the GI technique has been transferred to the time domain [20], [21] and spectral domain [22], [23], [24], demonstrating great potential in the applications of temporal waveform detection and spectroscopy, respectively. Similar theoretical analyses and experimental demonstrations show that the temporal GI has the same anti-scattering effect in the time domain, which leads to the progress of underwater wireless communication [25]. However, the properties have not been reported in the open-path spectroscopy in the frequency domain.

Here, based on computational spectral ghost imaging (CSGI) with Hadamard modulation, we propose a novel open-path ghost spectroscopy (GS) that can retrieve the spectral object through the strong turbulence path. In the proposed system, a programmable spectral filter is used to modulate a series of Hadamard patterns to a broadband signal provided by an amplified spontaneous emission (ASE) source, and the spectrum-under-test is recovered by cross correlation between the power measured by an optical power meter and the Hadamard patterns. Experimental results show that the spectral response of the object that transmitted through a 2-m long designed strong turbulence path can be reconstructed with the highest spectral resolution up to 0.126 nm.

This paper is organized as follows. In Section II, we introduce the principle of CSGI and explain the anti-turbulence characteristic of open-path GS. At the same time, the evaluation criterion for the GS results are also studied. In Section III, we establish the simulation system of CSGI based on Hadamard modulation, which obtains the ideal recovery performance of the system. In Section IV, we verify the proposed scheme through two experimental structures under the conditions of turbulence-free and strong turbulence, respectively, and analyze the different factors that affect the quality of the system. Finally, the main points of this article are summarized in Section V.

II. METHODS

A. Mathematical Principle of CSGI

From the phenomenon of two-photon entanglement to the architecture of computational GI with a single beam, GI is gradually getting rid of its mysterious appearance and revealing the essence of computational imaging: sampling and reconstructing of the target.

When using a structured light field as the sampling matrix, classical GI techniques can reconstruct the target according to

the covariance formula

$$Cov(X, Y) = E[(X - E(X)) \times (Y - E(Y))] \quad (1)$$

where $E(\cdot)$ represents taking the mean of element X or Y . Similarly, the spectral domain GI can be expressed as

$$O(\lambda) = \langle (B - \langle B \rangle) \times (I(\lambda) - \langle I(\lambda) \rangle) \rangle \quad (2)$$

where B represents the integral result obtained by the slow detector, $I(\lambda)$ is the reference structured light field, \times represents point-by-point multiplication, $\langle \cdot \rangle$ represents the average results of the multiple measurements. Due to the poor incoherence of the randomly distributed light field, there is high information redundancy between different detections, which will result in thousands of measurement times to achieve a good recovery, as described in [23]. Therefore, considering the single-arm CSGI technology with artificially coding structured light illumination is the way to relieve the computational resources consumption.

In CSGI, the intensity distribution of the detected spectral target at different frequency points is regarded as a one-dimensional array $\mathbf{F} = (f_1, f_2, \dots, f_m)$, and the broadband light source with specific spectral domain intensity distribution can also be regarded as a one-dimensional array $\mathbf{I}_N = (i_{N1}, i_{N2}, \dots, i_{Nm})$, where \mathbf{I}_N represents the distribution of the structured light field for the N_{th} time, $i_{N1}, i_{N2}, \dots, i_{Nm}$ represent the light field intensities at different frequency points relevant to the distribution in \mathbf{F} . When collecting the light intensity passing through the target with a slow detector, the corresponding mathematical representation is

$$\mathbf{B} = \mathbf{I}\mathbf{F} \quad (3)$$

where $\mathbf{I} = (\mathbf{I}_1, \mathbf{I}_2, \dots, \mathbf{I}_N)^T$ represents an $N \times m$ sampling matrix and $\mathbf{B} = (B_1, B_2, \dots, B_N)^T$ is a column vector composed of the results of N measurements of the slow detector. The recovery of \mathbf{F} can be expressed as

$$\mathbf{F} = \mathbf{I}^{-1}\mathbf{B} = \mathbf{I}^{-1}\mathbf{I}\mathbf{F} = \mathbf{E}\mathbf{F} \quad (4)$$

wherein \mathbf{I}^{-1} is the inverse of the sampling matrix and \mathbf{E} represents the identity matrix. (4) represents the reconstruction process of the target.

According to Eq. (4), when designing the structured light field with random modulation, like most cases in traditional GI system, the distributions of light sources often obey the Gaussian distribution matrix. Since the Gaussian distribution matrix is non-orthogonal, its covariance matrix will approach to the diagonal matrix only in the case of the measurement times N is much larger than the measurement points m , which explains the reason that the quality of GI reconstruction can be improved by increasing the number of detections.

On the other hand, when modulating the light field with an orthogonal matrix such as Hadamard matrix [26], any rows and columns of the matrix are orthogonal (incoherent), and any N_{th} order Hadamard matrix satisfies

$$\mathbf{H}^T\mathbf{H} = n\mathbf{E} \quad (5)$$

so that we can recover the high-quality target with only $N = m$ times of detection using the formula

$$\mathbf{F} = \mathbf{H}^T \mathbf{B} \quad (6)$$

Based on the aforementioned principle, in this paper, we also use Hadamard matrix to modulate the light. However, since the intensity distribution of light field is difficult to be directly expressed as +1 and -1, it is reasonable to decompose the Hadamard matrix into two matrices containing only 0 and 1, within which each of these rows separately corresponds to a group of Hadamard patterns to encode the light field

$$\begin{aligned} \mathbf{H}_N^+ &= (\mathbf{H}_N + 1) / 2 \\ \mathbf{H}_N^- &= 1 - \mathbf{H}_N^+ \end{aligned} \quad (7)$$

where \mathbf{H}_N^+ and \mathbf{H}_N^- represent a pair of complementary components of the Hadamard matrix. At the same time, when considering the random additive noise \mathbf{A}_{rand} in the actual transmission environment, the actual structured light field can be modified as

$$\begin{aligned} \mathbf{I}_N^+ &= \mathbf{H}_N^+ + \mathbf{A}_{rand} \\ \mathbf{I}_N^- &= \mathbf{H}_N^- + \mathbf{A}_{rand} \end{aligned} \quad (8)$$

where \mathbf{I}_N^+ and \mathbf{I}_N^- are the actual sampling matrices used to illuminate the target. Therefore, the form of the accumulated intensity in Eq. (3) can be written as

$$\begin{aligned} \mathbf{B}^+ &= \mathbf{I}_N^+ \mathbf{F} \\ \mathbf{B}^- &= \mathbf{I}_N^- \mathbf{F} \end{aligned} \quad (9)$$

Finally, when calculating $\mathbf{B} = \mathbf{B}^+ - \mathbf{B}^-$ and substituting it into Eq. (6) to reconstruct the target, the recovered spectrum $\mathbf{F} = \mathbf{H}_N^T \mathbf{B}$ without noise interference can be obtained.

In conclusion, Eqs. (3) and (4) unify the mathematical theory of CSGI, and also suggest that the way to achieve high-quality target recovery is to construct an orthogonal structured light field that can recover the identity matrix \mathbf{E} by certain times of matrix operation.

B. Theoretical Analysis of Anti-Turbulence Properties for GS

It is well known that open-path laser beam can be affected by the atmospheric turbulence and near-field airflow effect, which is specifically appeared as the intensity fluctuation, phase fluctuation, beam expansion, beam drift, and image point jitter caused by the changes in the refractive index of atmospheric molecular clusters. In addition to the influence on the spatial distribution of the light field, turbulence effect can also lead to the drift and distortion of the laser beam spectrum, which will affect the measurement accuracy of the optical spectrum analyzer (OSA). According to [27], the expression of the spectrum of Gaussian beams transmitted through the atmosphere is given by

$$\begin{aligned} S(x, z, \omega) &= S^0(\omega) \left[\frac{k}{2z\beta_1\beta_2} \right] \times \exp \left[-\frac{k^2}{2z^2\beta_1^2\beta_2^2} \frac{x^2}{w_0^2} \right] \\ \beta_1^2 &= \frac{1}{w_0^2} + \frac{1}{\rho_0^2} - i \frac{k}{2z} \\ \beta_2^2 &= \frac{1}{w_0^2} + \frac{1}{\rho_0^2} + i \frac{k}{2z} - \frac{1}{\beta_1^2 \rho_0^4} \end{aligned}$$

$$\rho_0 = (0.545 C_n^2 k^2 z)^{-3/5} \quad (10)$$

where $S^0(\omega)$ is the transmitted laser spectrum, C_n^2 represents the refractive-index structure constant which expresses the degree of turbulence, k is the wavenumber, and w_0^2 represents the radius of waist spot of the laser beam. (10) shows that the intensity of the spectrum can be collectively affected by the transmission distance, turbulence intensity, spectral bandwidth, off-axis position, and the beam waist, which will lead to the drift distortion of the spectrum.

The proposed GS can conditionally eliminate the effect of atmospheric turbulence. During the detection of GS, when the turbulence path is before the target, the spectrum distribution of the structured light field will be distorted by the turbulence effect. The corresponding detection intensity can be expressed as

$$\mathbf{B} = \int |S(x, z, \lambda)|^2 \mathbf{F}(\lambda) d\lambda \quad (11)$$

where $S(x, z, \lambda)$ is the structured light field influenced by the turbulence path. Since the original structured light field used to recover the target is $S^0(\lambda)$, the target recovery quality will be reduced due to the deviation between $S^0(\lambda)$ and $S(x, z, \lambda)$ when substituting $S^0(\lambda)$ into the cross-correlation formula. However, the quality of the recovery can be improved to some extent by increasing the measurement times or setting a reference beam to detect the spectrum $S(x, z, \lambda)$ and eliminate the turbulence effect through cross correlation between two beams that experience the same turbulence [28].

When the turbulence path is behind the target, the spectrum recovery will not be affected, since the structured light field $S^0(\lambda)$ keeps unchanged and the accumulated intensity of the spectrum is consistent with the turbulence-free situation when ignoring the effect of turbulence on photon number. Therefore, the corresponding detection intensity can be expressed as

$$\mathbf{B} = \int |S^0(\lambda)|^2 \mathbf{F}(\lambda) d\lambda \quad (12)$$

C. Evaluation Criterion for GS Results

To evaluate the quality of the GS, the signal-to-noise ratio (SNR) is defined as [21]

$$SNR = 10 \log \frac{\sum_{i=1}^N (F(i) - \bar{F})^2}{\sum_{i=1}^N (G(i) - F(i))^2} \quad (13)$$

where $G(i)$ and $F(i)$ respectively represent the recovered spectrum and the original target spectrum, $\bar{F} = \sum_{i=1}^N F_i / N$.

In the actual experiment, the SNR of the recovered spectrum by GS is dependent on lots of environmental factors, including turbulence transmission path, modulation precision of programmable filter, disturbance from optical fiber, and so on. Specific analysis of the SNR of the GS and the corresponding improvement methods will be discussed in Section IV.

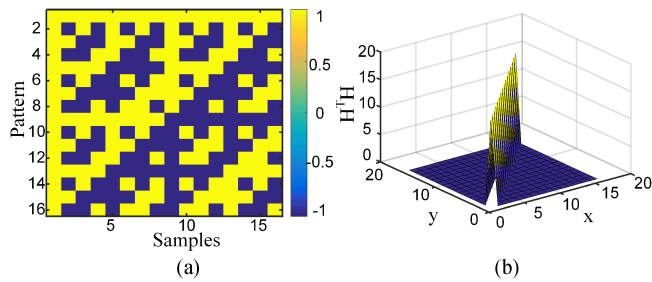


Fig. 2. (a) 16×16 Hadamard matrix composed of +1 (yellow) and -1 (blue) elements. (b) the orthogonality verification of Hadamard sampling matrix with $H^T H$.

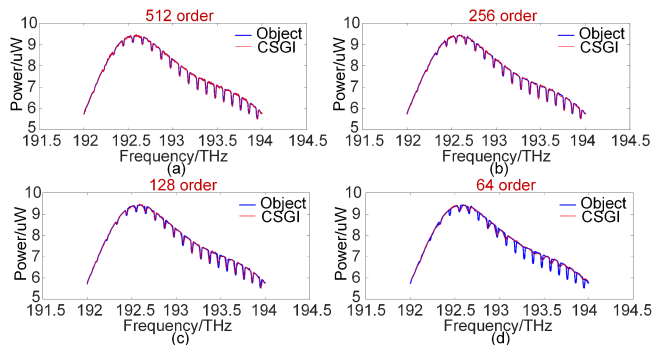


Fig. 3. Simulation results of CSGI with different measurement times: (a) 512, (b) 256, (c) 128, and (d) 64.

III. NUMERICAL STUDY

In the first step, a simulation is carried out. Fig. 2 shows the composition and orthogonality verification of the 16-order Hadamard matrix we used in our simulation. The elements in yellow and blue in Fig. 2(a) respectively represent the +1 and -1 elements in the Hadamard matrix. The result in Fig. 2(b) is the cross correlation between different rows and columns in the Hadamard matrix, showing that each row and column in the matrix is only related to itself. Based on this kind of Hadamard modulation, actual sampling matrices I_N^+ and I_N^- of order 512, 256, 128, and 64 are built, according to (8). Then, a known absorption spectrum of a hydrogen cyanide gas cavity with a data length of $m = 512$ is chosen as the spectral target under test. When multiplying the spectral target (that is correspondingly down-sampled to meet the requirements of matrix multiplication dimension) with the actual sampling matrices, the measurement results can be obtained as described in (6). The recovered absorption spectrum of the hydrogen cyanide gas cavity with different measurement times (i.e., the order of the matrix) are compared and shown in Fig. 3, where the blue line represents the spectral target to be measured, and the red line represents the recovered spectrum by CSGI. It can be seen that the shape of the gas absorption spectrum can still be distinguished even with only 64 measurements, which is almost impossible for the GI with random modulation. At the same time, when the number of measurements is increased from 64 to 512, the quality of spectrum recovery is significantly improved. Furthermore, according to the SNR definition in (13), the SNR in different conditions is also analyzed and shown in Fig. 4. As can be seen

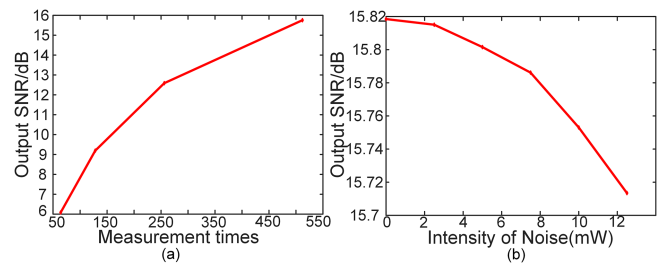


Fig. 4. SNR analysis of the simulation CSGI system with the increase of (a) Measurement times and (b) Intensity of noise.

TABLE I
SNR AND MEASUREMENT SPEED OF CSGI UNDER DIFFERENT MEASUREMENT TIMES

Measurement times	512	256	128	64
SNR/dB	15.8	12.6	9.2	6.1
Time/ms	2.33	0.83	0.67	0.47

from Fig. 4(a), when the noise level keeps constant, increasing the measurement times can improve the SNR of the system, but the rate of rising slope decreases gradually. Besides, Fig. 4(b) shows that when the measurement times keep at 512, the SNR will be gradually reduced by increasing the noise level, but it remains at a high level above 15.7 dB, showing a good spectral detection performance.

We also analyze the measurement speed under different measurement times as shown in Table I. As can be seen from the table, larger measurement times correspond to higher SNR but longer recovery time. It should be noted that although a better recovery effect can also be achieved by the conventional spectral domain GI, it requires tens of thousands of calculations to process a larger amount of data [23], which shows again that the advantage of CSGI in saving time sources compared with the traditional counterpart.

IV. EXPERIMENTAL STUDIES AND DISCUSSION

A. Experimental Setup of All Fiber-Based GS

Based on the principle and simulation results of the proposed CSGI system, an all fiber-based GS is firstly constructed as illustrated in Fig. 5. A section of the ASE source provided by an erbium-doped fiber amplifier (EDFA) is served as a broad-spectrum light covering the frequency range of 192-194 THz. When the broad light passes through a programmable spectral filter, the light field at different frequency points is modulated. The spectral-targets-under-test in the experiment is a reconfigurable optical filter provided by another programmable spectral filter. In order to get the accumulated intensity after the spectral target, an optical power meter is used. When feeding different Hadamard patterns into the programmable spectral filter in sequence, a series of integral intensities can correspondingly be obtained, which can then be substituted into (6) with the Hadamard patterns to restore the spectral targets.

The normalized spectra of three different spectral targets by using a 32-order Hadamard matrix are presented in Fig. 6. As can

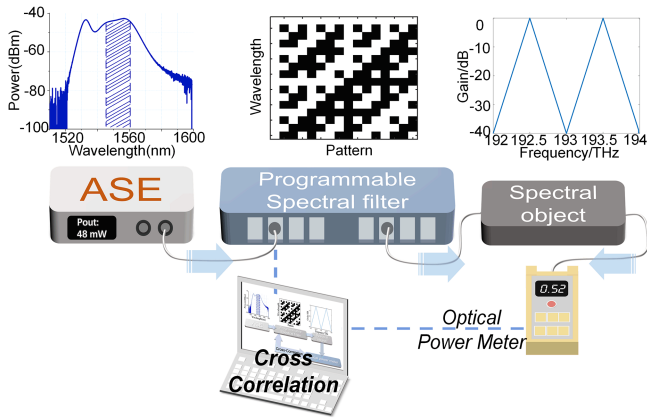


Fig. 5. Experimental setup of the fiber-based GS. The spectrum selected from the ASE source is highlighted in the shadow area.

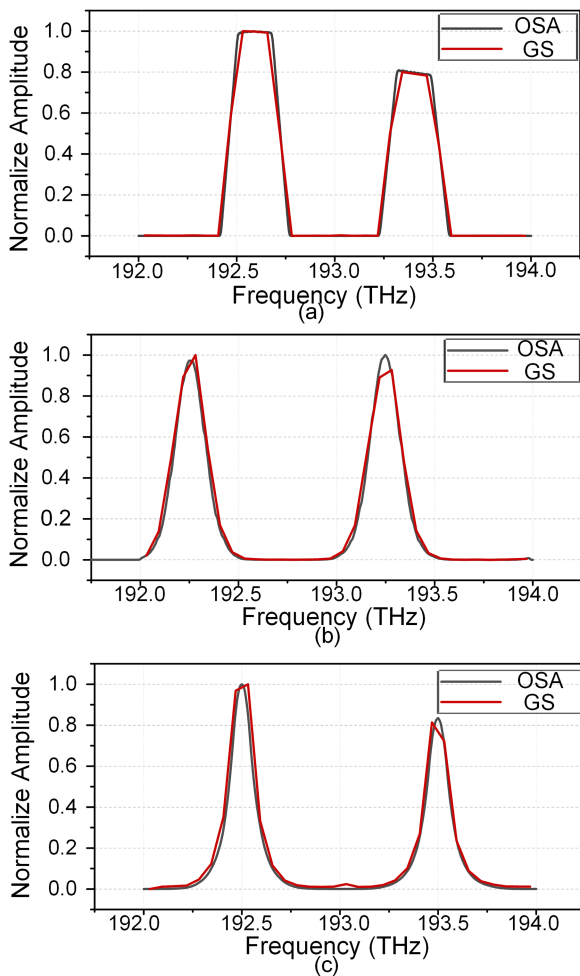


Fig. 6. The retrieved spectra of (a) square-, (b) Sine-, and (c) Triangle-shaped targets by the fiber-based GS (red line) and OSA (black line).

be seen, the retrieved spectra by the proposed GS (red line) match well with the results directly measured by an OSA (black line). The results show that, by using only 64 times of measurements, the GS still has the ability to reconstruct different shapes of spectral objects in a wide frequency range with high quality.

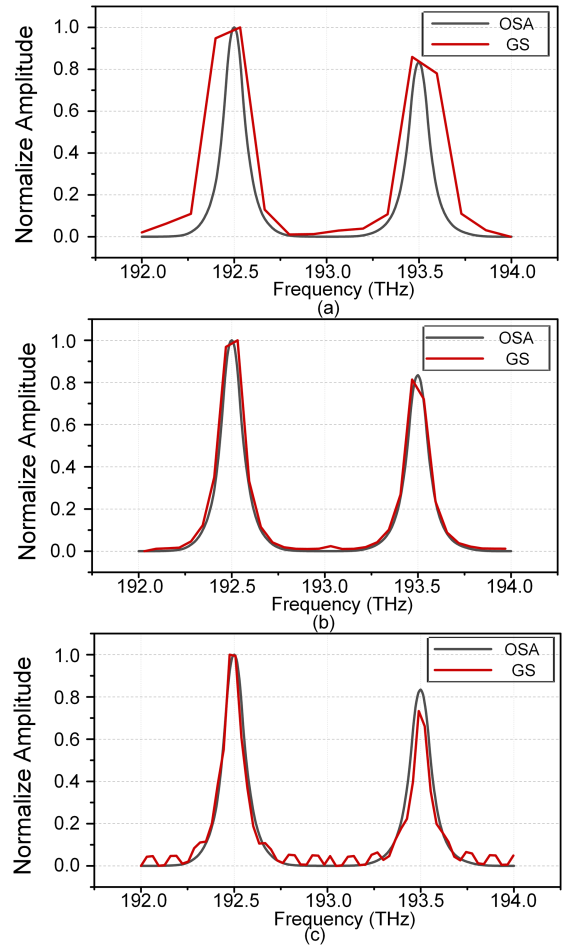


Fig. 7. The spectra of the triangle-shaped target with (a) 16-, (b) 32-, and (c) 64-times of measurements by the proposed GS (Red line) and OSA (black line).

And since the switching time of each pattern is 500ms, the whole process takes 32 s.

Subsequently, another experiment is carried out to test the system performance under different measurement times by modulating the light field with 16-, 32- and 64-order of Hadamard matrix. The corresponding recovered triangle-shaped optical spectra are depicted as the red lines in Fig. 7. As can be seen from Fig. 7(a), although the recovered result still fits the reference spectrum obtained by the OSA (black line), the quality of the recovered spectrum with only 16 times of measurements is the worst, which can only roughly identify the shape of the spectral target, with an SNR of -13.3111 dB. The spectrum with 32 times of measurements in Fig. 7(b) has a higher quality, and the SNR is significantly increased to 36.1814 dB. This is because more frequency points are sampled in the same frequency range, which leads to a more accurate restoration. However, different with the simulation results, the recovery quality does not simply improve when using the 64-order of Hadamard matrix, which is depicted in Fig. 7(c). Although the high intensity part of the recovered spectrum fits the reference spectrum better, the part with low intensity appears large spectrum distortion with a zigzag shape, and the corresponding SNR degenerates to 28.5029 dB. The reason for the deterioration can be attributed to the distortion

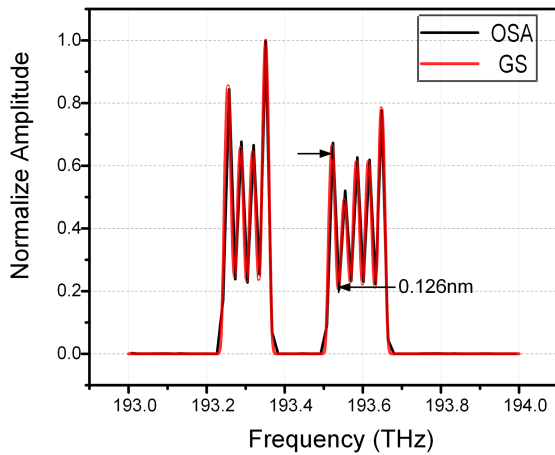


Fig. 8. The experimental retrieved spectra with a characteristic spectral fluctuation of 0.126 nm. Red line: measurements by GS, black line: measurements by OSA.

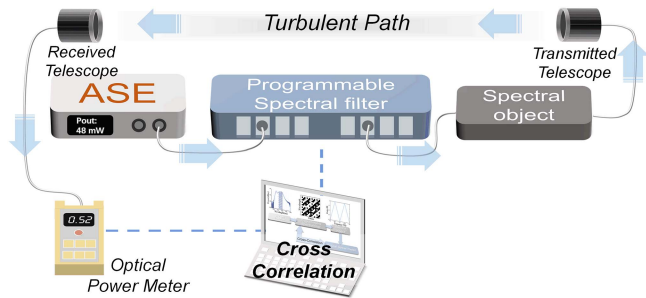


Fig. 9. Experimental setup of the open-path GS.

of the structured light field because of the limited resolution of the programmable spectral filter (i.e., 1 GHz in the experiment). The detailed analysis will be given in the *Results and Discussion* part.

Nevertheless, in order to test the highest resolution of the system, a spectral target in the frequency range of 193-194 THz with a characteristic spectral fluctuation of 0.126 nm is recovered, which is illustrated in Fig. 8. Again, due to the limited resolution of the programmable spectral filter, we choose the 64-order Hadamard matrix to modulate the light source in this 1 THz range, which corresponds to an average sampling of 64 points in this spectrum. As can be seen, the recovered spectrum by the proposed GS (red line) still fits well with the direct measurement by the OSA (black line), which shows that the spectral resolution of our GS can reach 0.126 nm.

B. Experimental Setup of GS in Turbulence Environment

In addition to the fiber-based GS, an open-path GS, as shown in Fig. 9, is further constructed to verify the anti-turbulence effect. By replacing the fiber between the spectral target and optical power meter with a pair of telescopes, a 2-m long open path with strong turbulence is built up by a hairdryer (strong wind and air heating). The same triangular-shaped spectral target is also used for the performance comparison. As can be seen from the spectra measured by the OSA in the turbulence-free (black line) and strong turbulence (blue line) environments in Fig. 10, the

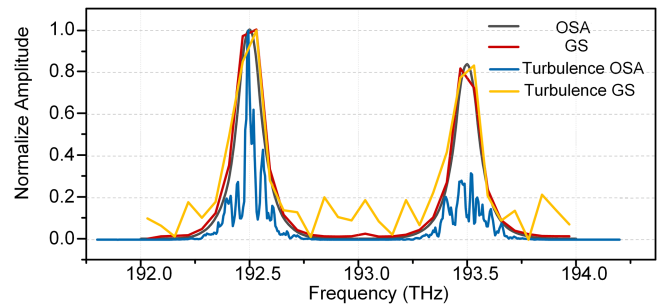


Fig. 10. Comparison of the retrieved triangle-shaped spectra in turbulence-free and strong turbulence environments. Direct measurements by OSA with (blue) and without (black) turbulence. Measurements by the proposed GS with (yellow) and without (red) turbulence.

latter is wildly fluctuated and almost indistinguishable, which demonstrates that the conventional OSA-based method cannot directly be employed to achieve open-path spectroscopy in the strong turbulence environment.

In the proposed GS, the structured light field is modulated by a 32-order Hadamard matrix, and the measured spectra are also presented in Fig. 10. As can be seen from the recovered spectrum in the turbulence-free environment (red line), it fits well with the spectrum directly measured by OSA. More importantly, the recovered spectrum in the strong turbulence environment (yellow line) still shows the same clear curve with the reference spectrum, which proves the anti-turbulence ability of the GS in the open path. Therefore, the results show that the proposed open-path GS can work well in both the turbulence-free and strong turbulence environments.

C. Results and Discussion

In this part, we will discuss different factors that would influence the quality of the proposed open-path GS.

Firstly, as mentioned in Section IV, although more measurement times ideally mean better recovery performance, the GS recovery quality cannot be improved by simply increasing the measurement times. The spectrum detection resolution of the system depends on the upper limit of the spectral modulation capability, which can be expressed as

$$O(\Delta\lambda) = \langle (B - \langle B \rangle) \times (I(\Delta\lambda) - \langle I(\Delta\lambda) \rangle) \rangle \quad (14)$$

where $\Delta\lambda$ represents the minimum spectral characteristic fluctuation, which can also be regarded as the spectral resolution. Eq. (14) is the variant of Eq. (2). This formula proves that the minimum spectral fluctuation of the target spectrum $O(\Delta\lambda)$ merely influenced by the resolution of the coding pattern $I(\Delta\lambda)$, that is to say, limited by the spectral manipulation resolution of the programmable spectral filter.

Secondly, due to the air heating condition, the thermal noise in the open path is relatively large. It will drown out the portion of the target spectrum under the extremely low-level light intensity conditions, leading to the reduction of the overall intensity to about -30.51 dBm in the strong turbulence environment. Furthermore, the heating environment will introduce the random motion of photons, which will increase the fluctuation of the intensity

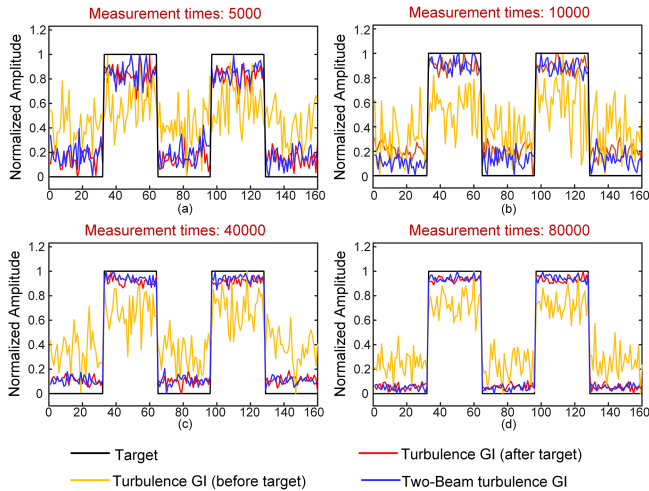


Fig. 11. Simulation results of GS in different turbulence situations and different measurement times (a) 5000, (b) 10000, (c) 40000, (d) 80000. Black line: spectral target, red line: GS when turbulence path after the target, yellow line: GS when turbulence path before the target, blue line: two-beam GS when turbulence path before the target.

detected by the optical power meter. This explains why there exists large amplitude fluctuation at the bottom of the spectrum, as the yellow line shows in Fig. 10.

Thirdly, the effect of turbulence on the proposed GS system (especially when the turbulence path is before the target) is verified by simulation as shown in Fig. 11. In the simulation, the spectral target (black line) is illuminated with a Gaussian pseudo-random distribution matrix. The turbulence effect on the spectral illuminating field is simulated by superimposing a random noise matrix on the Gaussian irradiation matrix. As can be seen, when the turbulence path exists after the target, the recovered ghost images (red line) fit well with the spectral target. This is because the turbulence effect after the target will not influence the accumulated intensity as well as the illuminating field. However, when the turbulence path exists before the target, since the illuminating field is strongly influenced by the turbulence effect, the recovered ghost images (yellow line) are almost indistinguishable.

Besides, in order to demonstrate the anti-turbulence imaging based on a reference beam, a two-beam spectral domain GI structure (blue lines) is also simulated. As can be seen, by adding a reference beam, the simulation results obtained by the two-beam structure match well with the spectral target as well. This is because the reference beam can directly detect the noised-influenced illuminating field and retrieve the ghost image with this illuminating field distribution. Therefore, the turbulence effect can be eliminated, or even enhance the randomness of the spectral illuminating field.

At the same time, the recovered ghost images under different turbulence situations with different measurement times are also compared and shown in Fig. 11. When the measurement times increase from 5000 to 80000, the qualities of the recovered ghost images are improved in all situations, even in seriously turbulence-influenced condition.

Fourthly, the recovery quality will also be influenced by the spectral shape distortion induced by different transmission

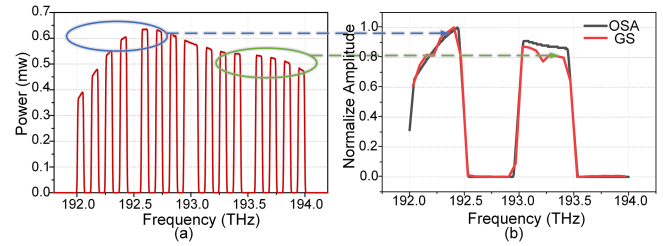


Fig. 12. (a) Hadamard pattern and (b) Recovered spectra influenced by the spectrum envelope of EDFA.

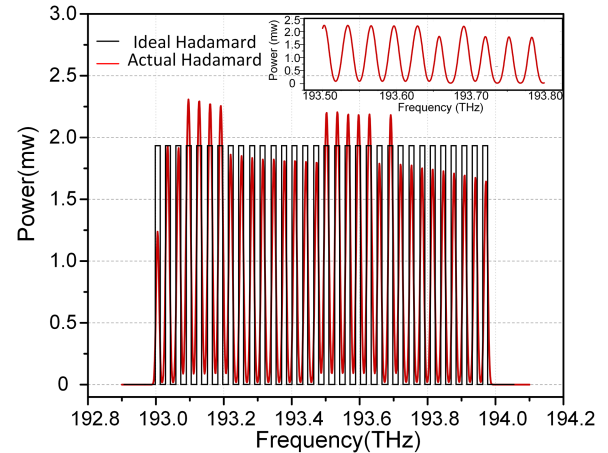


Fig. 13. Distortion of the Hadamard pattern due to the limited resolution of programmable spectrum filter. Black line: ideal Hadamard pattern, red line: actual Hadamard pattern with distortion. Inset figure: the zoom-in view of the Hadamard pattern within the range of 193.5-193.8 THz.

characters of the equipment in the system. For example, the unflatness of the spectrum envelope of EDFA will cause the distortion of the Hadamard modulated spectrum. As shown in Fig. 12(a), it exhibits the envelope distortion of a certain kind of Hadamard pattern. Fig. 12(b) shows the recovered results affected by the same fluctuation at the corresponding frequency point. This problem can be solved by introducing a spectrum flattening mechanism to compensate the spectral fluctuation at different frequency points.

Fifthly, the programmable spectral filter will also induce a certain degree of distortion to the Hadamard pattern as shown in Fig. 13. The black line represents the ideal Hadamard pattern, and the red line represents the actual Hadamard pattern. As can be seen, except for the huge amplitude fluctuation of the whole envelope, the Hadamard pattern is also largely deteriorated to make it almost impossible to distinguish the adjacent rectangle shape of the matrix elements, which can lead to serious distortion of the actual recovery results.

Therefore, in order to improve the spectral resolution in future research, a possible way is to replace the programmable spectral filter with other modulation methods to achieve more sophisticated spectral operations, or to replace the Hadamard matrix with other orthogonal coding methods to avoid the requirements for 0-1 amplitude waveform modulation. Besides, in order to reduce the modulation time, a more efficient way of multiplexing to

TABLE II
COMPARISON BETWEEN THE PROPOSED GS WITH COMMERCIAL OSA

	Commercial OSA	Proposed GS
Resolution	0.1 nm	0.125 nm
Measurement bandwidth	600-1700 nm	1530-1563 nm
Measurement speed	0.2 s	32 s
Dynamic range	71 dB	38.2 dB
cost	40000 dollars	60000 dollars
Anti-turbulence characteristic	no	Yes

achieve one-shot detection of the time-varying spectral targets is also desirable.

At last, an objective and comprehensive comparison between the proposed GS system and the commercial OSA (YOKO-GAWA, AQ6370D) is listed in Table II. As can be seen, for a newborn spectroscopy method, the measurement performances of the proposed GS system seem not good enough, which cannot compete with the mature spectrometer products that have been developed for decades. However, it should be noted that the performances of the proposed GS, such as the highest frequency setting resolution, operating frequency range, filter control setting time, optical power limitation and cost, are mainly limited by the programmable spectral filter in the structure. As a result, by using the new spectral modulation technology to replace the programmable spectral filter, for example, an integrated waveshaper [29] or optical phased array [30], the cost of the proposed GS system is expected to be largely reduced and a breakthrough in the system performances can be achieved as well.

V. CONCLUSION

In this paper, we analyze the principle and anti-turbulence property of GI in the spectral domain, and propose an open-path GS based on CSGI technology. Experimental results show that the proposed GS can achieve a spectral resolution of up to 0.126 nm in the range of 192-194 THz with only 64 times of measurements. Besides, it also verifies a good recovery performance with a 2-m long strong turbulence path. Compared with other open-path spectroscopy technologies, the proposed technique can realize the spectrum recovery in the condition of weak light and strong turbulence at a low detection cost, which may find applications in greenhouse gas detection and remote sensing communication in the open path.

REFERENCES

- [1] J. K. Hedelius et al., "Southern California megacity CO₂, CH₄, and CO flux estimates using ground- and space-based remote sensing and a Lagrangian model," *Atmospheric Chem. Phys.*, vol. 18, no. 22, pp. 16271–16291, Nov. 2018.
- [2] G. B. Rieker et al., "Frequency-comb-based remote sensing of greenhouse gases over kilometer air paths," *Optica*, vol. 1, no. 22, pp. 290–298, Oct. 2014.
- [3] K. C. Cossel et al., "Open-path dual-comb spectroscopy to an airborne retroreflector," *Optica*, vol. 4, no. 7, pp. 724–728, Jun. 2017.

- [4] D. W. T. Griffith, D. Pöhler, S. Schmitt, S. Hammer, S. N. Vardag, and U. Platt, "Long open-path measurements of greenhouse gases in air using near-infrared Fourier transform spectroscopy," *Atmospheric Meas. Techn.*, vol. 11, no. 3, pp. 1549–1563, Mar. 2018.
- [5] B. Byrne et al., "Monitoring urban greenhouse gases using open-path fourier transform spectroscopy," *Atmos. Ocean.*, vol. 58, no. 1, pp. 25–45, Feb. 2020.
- [6] L. M. Wang, Y. J. Zhang, H. B. Li, Y. Zhou, and W. Q. Liu, "Effect of turbulence on laser absorption signal and its improvement method," *Laser Technol.*, vol. 36, no. 5, pp. 670–673, Sep. 2012.
- [7] T. B. Pittman, Y. H. Shih, D. V. Strekalov, and A. V. Sergienko, "Optical imaging by means of two-photon quantum entanglement," *Phys. Rev. A*, vol. 52, no. 5, pp. R3429–R3432, Nov. 1995.
- [8] J. H. Shapiro, "Computational ghost imaging," *Phys. Rev. A*, vol. 78, no. 6, Dec. 2008, Art. no. 061802.
- [9] Y. Bromberg, O. Katz, and Y. Silberberg, "Ghost imaging with a single detector," *Phys. Rev. A*, vol. 79, no. 5, May 2009, Art. no. 053840.
- [10] B. Sun, S. S. Welsh, M. P. Edgar, J. H. Shapiro, and M. J. Padgett, "Normalized ghost imaging," *Opt. Exp.*, vol. 20, no. 15, pp. 16892–16901, Jul. 2012.
- [11] O. Katz, Y. Bromberg, and Y. Silberberg, "Compressive ghost imaging," *Appl. Phys. Lett.*, vol. 95, no. 13, Sep. 2009, Art. no. 131110.
- [12] Z. Zhang, X. Ma, and J. Zhong, "Single-pixel imaging by means of Fourier spectrum acquisition," *Nat. Commun.*, vol. 6, no. 1, pp. 1–6, Feb. 2015.
- [13] Z. Zhang, X. Wang, G. Zheng, and J. Zhong, "Hadamard single-pixel imaging versus Fourier single-pixel imaging," *Opt. Exp.*, vol. 25, no. 16, pp. 19619–19639, Aug. 2017.
- [14] M. Bina, D. Magatti, M. Molteni, A. Gatti, L. A. Lugiato, and F. Ferri, "Backscattering differential ghost imaging in turbid media," *Phys. Rev. Lett.*, vol. 110, no. 8, Feb. 2013, Art. no. 083901.
- [15] V. Durán et al., "Compressive imaging in scattering media," *Opt. Exp.*, vol. 23, no. 11, pp. 14424–14433, May 2015.
- [16] R. E. Meyers, K. S. Deacon, and Y. Shih, "Turbulence-free ghost imaging," *Appl. Phys. Lett.*, vol. 98, no. 11, Mar. 2011, Art. no. 111115.
- [17] R. E. Meyers, K. S. Deacon, and Y. Shih, "Positive-negative turbulence-free ghost imaging," *Appl. Phys. Lett.*, vol. 100, no. 13, Mar. 2012, Art. no. 131114.
- [18] P. Zhang, W. Gong, X. Shen, and S. Han, "Correlated imaging through atmospheric turbulence," *Phys. Rev. A*, vol. 82, no. 3, Sep. 2010, Art. no. 033817.
- [19] M. Chen et al., "Ghost imaging lidar via sparsity constraints in real atmosphere," *Opt. Photon. J.*, vol. 3, no. 2, pp. 83–85, Jun. 2013.
- [20] P. Ryczkowski, M. Barbier, A. T. Friberg, J. M. Dudley, and G. Genty, "Ghost imaging in the time domain," *Nat. Photon.*, vol. 10, no. 3, pp. 167–170, Feb. 2016.
- [21] J. Tang, D. Zou, M. Cheng, L. Deng, D. Liu, and M. Zhang, "Single-shot temporal ghost imaging based on orthogonal frequency-division multiplexing," *IEEE Photon. Technol. Lett.*, vol. 30, no. 17, pp. 1555–1558, Sep. 2018.
- [22] P. Janassek, S. Blumenstein, and W. Elsässer, "Ghost spectroscopy with classical thermal light emitted by a superluminescent diode," *Phys. Rev. Appl.*, vol. 9, no. 2, Feb. 2018, Art. no. 021001.
- [23] C. Amiot, P. Ryczkowski, A. T. Friberg, J. M. Dudley, and G. Genty, "Supercontinuum spectral-domain ghost imaging," *Opt. Lett.*, vol. 43, no. 20, pp. 5025–5028, Oct. 2018.
- [24] P. Ryczkowski, C. G. Amiot, J. M. Dudley, and G. Genty, "Experimental demonstration of spectral domain computational ghost imaging," *Sci. Rep.*, vol. 11, no. 1, pp. 1–7, Apr. 2021.
- [25] X. Chen et al., "Computational temporal ghost imaging for long-distance underwater wireless optical communication," *Opt. Lett.*, vol. 46, no. 8, pp. 1938–1941, Apr. 2021.
- [26] J. Zhao, Z. Tang, K. Shao, and S. Pan, "Computational spectral-domain ghost imaging based on Hadamard modulation," in *Proc. IEEE Int. Topical Meeting Microw. Photon.*, Matsue, Japan, 2020, pp. 253–255.
- [27] S. Xueju, W. Long, S. Hongbin, and H. Yudong, "Propagation analysis of flattened circular Gaussian beams with a misaligned circular aperture in turbulent atmosphere," *Opt. Commun.*, vol. 282, no. 24, pp. 4765–4770, Dec. 2009.
- [28] Y. Shih, "The physics of turbulence-free ghost imaging," *Technologies*, vol. 4, no. 4, Dec. 2016, Art. no. 4040039.
- [29] S. Zheng et al., "Chip-scale reconfigurable optical full-field manipulation: Enabling a compact grooming photonic signal processor," *ACS Photon.*, vol. 7, no. 5, pp. 1235–1245, Jul. 2020.
- [30] K. Komatsu, Y. Ozeki, Y. Nakano, and T. Tanemura, "Ghost imaging using integrated optical phased array," in *Proc. IEEE Opt. Fiber Commun. Conf. and Exhib.*, CA, USA, 2017, pp. 1–3.

Jianing Zhao received the B.S. degree, in 2019, in electronic and information engineering from the Nanjing University of Aeronautics and Astronautics, Nanjing, China, where she is currently working toward the Ph.D. degree with the Key Laboratory of Radar Imaging and Microwave Photonics, Ministry of Education. Her research interests include computational imaging, optical communication, and microwave photonic measurement.

Fengyuan Liu received the B.S. degree, in 2021, in electronics engineering from the Nanjing University of Aeronautics and Astronautics, Nanjing, China, where he is currently working toward the M.S. degree with the Key Laboratory of Radar Imaging and Microwave Photonics, Ministry of Education. His research interests include microwave photonic communication and beamforming technology.

Zhenzhou Tang (Member, IEEE) received the M.S. degree in information engineering, the Ph.D. degree in communication and information system, from the Nanjing University of Aeronautics and Astronautics (NUAA), Nanjing, China, in 2014 and 2019, respectively, and the second Ph.D. degree in photonics engineering from Ghent University, Ghent, Belgium, in 2020. He is currently an Associate Professor with the Key Laboratory of Radar Imaging and Microwave Photonics, Ministry of Education, NUAA. He has authored or coauthored more than 40 research papers, including more than 15 papers in peer-reviewed journals and 15 papers in conference proceedings. His research interests include photonics-based microwave mixing, photonic integrated circuits, and radio over fiber communications. He is one of the recipients of the 2017 IEEE Photonics Society Graduate Student Fellowship. He is also the Affiliated Member of IEEE MTT-S Microwave Photonics Committee.

Shilong Pan (Senior Member, IEEE) received the B.S. and Ph.D. degrees in electronic engineering from Tsinghua University, Beijing, China, in 2004 and 2008, respectively. From 2008 to 2010, he was a Vision 2010 Postdoctoral Research Fellow with the Microwave Photonics Research Laboratory, University of Ottawa, ON, Canada. He joined the College of Electronic and Information Engineering, Nanjing University of Aeronautics and Astronautics, Nanjing, China, in 2010, where he is currently a Full Professor and an Executive Director of the Key Laboratory of Radar Imaging and Microwave Photonics, the Ministry of Education. Prof. Pan has authored or coauthored more than 400 papers in peer-reviewed journals and conference proceedings. His research has focuses on microwave photonics, which include optical generation and processing of microwave signals, analog photonic links, photonic microwave measurement, and integrated microwave photonics. Prof. Pan is an Associate Editor for JOURNAL OF LIGHTWAVE TECHNOLOGY, ELECTRONICS LETTERS, and PHOTONIX, and the Deputy Editor of CHINESE OPTICS LETTERS. He is also the Vice Chair of IEEE MTT-22 MICROWAVE PHOTONICS. Prof. Pan was a Chair of a number of international conferences, symposia, and workshops, including the TPC Chair of ICOCN 2015, TPC Co-chair of IEEE MWP 2017, and the General Co-chair of IEEE MWP 2021. Prof. Pan is a Fellow of OSA, SPIE and IET. He was selected as an IEEE Photonics Society Distinguished Lecturer, in 2019 and was the recipient of IEEE MTT-S Outstanding Young Engineer Award, in 2021.